PHYSICAL REVIEW B VOLUME 61, NUMBER 19 15 MAY 2000-I

Far-infrared vibrational properties of high-pressure high-temperature C_{60} polymers and the C_{60} dimer

V. C. Long and J. L. Musfeldt
Department of Chemistry, State University of New York at Binghamton, Binghamton, New York 13902-6016

K. Kamarás
Research Institute for Solid State Physics and Optics, Hungarian Academy of Sciences, H-1525 Budapest, Hungary

G. B. Adams and J. B. Page
Department of Physics and Astronomy, Arizona State University, Tempe, Arizona 85287

Y. Iwasa
Japan Advanced Institute of Science and Technology, Tatsunokuchi, Ishikawa 923-1292, Japan

W. E. Mayo
Department of Ceramic and Materials Engineering, Rutgers University, Piscataway, New Jersey 08854-8065

(Received 8 December 1999)

We report high-resolution far-infrared transmission measurements of the $2+2$ cycloaddition C_{60} dimer and two-dimensional rhombohedral and one-dimensional orthorhombic high-pressure high-temperature C_{60} polymers. In the spectral region investigated (20–650 cm^{-1}), we see no low-energy interball modes, but symmetry breaking of the linked C_{60} balls is evident in the complex spectrum of intramolecular modes. Experimental features suggest large splittings or frequency shifts of some I_hC_{60}-derived modes that are activated by symmetry reduction, implying that the balls are strongly distorted in these structures. We have calculated the vibrations of all three systems by first-principles quantum molecular dynamics and use them to assign the predominant I_hC_{60} symmetries of observed modes. Our calculations show unprecedentedly large downshifts of $T_{1u}(2)$-derived modes and extremely large splittings of other modes, both of which are consistent with the experimental spectra. For the rhombohedral and orthorhombic polymers, the $T_{1u}(2)$-derived mode that is polarized along the bonding direction is calculated to downshift below any $T_{1u}(1)$-derived modes. We also identify a previously unassigned feature near 610 cm^{-1} in all three systems as a widely split or shifted mode derived from various silent I_hC_{60} vibrations, confirming a strong perturbation model for these linked fullerene structures.

I. INTRODUCTION

The molecular nature of solid C_{60} is apparent in its exceptionally simple vibrational spectrum, which exhibits four sharp infrared (IR) modes, as expected for an isolated cage of icosahedral symmetry.[1,2] When the weak van der Waals forces among fullerene balls are replaced by different configurations of covalent bonds, the vibrational properties change dramatically.[3–5] Both interball interactions and symmetry reductions produced by distortions of the bonded C_{60} balls are effectively studied through their effects on the vibrational spectrum.

C_{60} is known to form two types of polymer connections. Neutral C_{60}'s polymerize by forming between one and six $2+2$ cycloaddition interball connections, in which parallel 6-6 bonds on adjacent C_{60}'s are connected by a pair of carbon-carbon (C-C) bonds. (See Fig. 1.) Charged C_{60}'s polymerize with the same $2+2$ cycloaddition connections, or by forming atom-atom connections, each consisting of one C-C bond between neighboring C_{60}'s. The observed polymerized C_{60} structures include dimers[6,7] orthorhombic one-dimensional (1D) chains,[8–10] tetragonal and rhombohedral two-dimensional (2D) lattices,[4,11] and some disordered 3D structures,[12] among others.[13] Methods of preparing the $2+2$ cycloaddition dimer include mechanochemical reaction of C_{60} with KCN or Li,[7,14] high-temperature phototransformation,[15] quasihydrostatic compression,[16] and pressurization of the template compound $(ET)_2C_{60}$.[17] Room-temperature exposure of C_{60} to visible or ultraviolet light creates a disordered array of small closed oligomers, referred to as the photopolymer.[13] The extended $2+2$-connected structures (1D, 2D, and 3D) can be made with neutral C_{60}'s

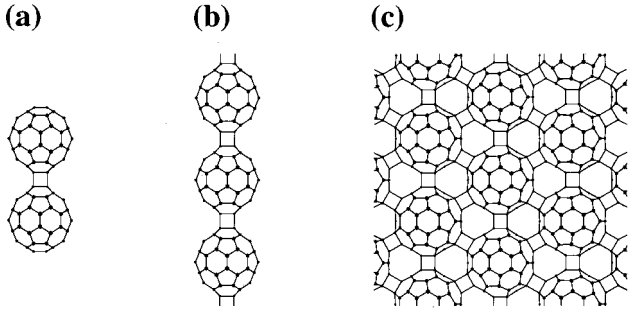

FIG. 1. Structures of the (a) dimer, (b) *O* polymer, and (c) *R* polymer.

under a variety of high-pressure high-temperature (HPHT) conditions.[18] In addition, the 2+2-connected 1D orthorhombic chains can be made with charged C_{60}'s by intercalation of C_{60} with alkali-metal ions (A_nC_{60} with $n=1$).[8,9] These charged 1D chains are structurally indistinguishable, by x-ray diffraction,[10,19] from the neutral 1D chains made by HPHT processes. Finally, the charged C_{60} dimer with an atom-atom connection may be made by quenching AC_{60},[6] and more exotic atom-atom phases have been created in Na_4C_{60} and Na_2RbC_{60}.[11,20]

Vibrational spectroscopy is well suited to the study of molecular symmetry and symmetry reductions, and has been used extensively to investigate C_{60} and fullerene-derived materials.[2,21,22] To date, however, no complete identification of experimental modes has been attempted for the vibrational spectrum of any polymerized fullerene.[18] In the linked fullerene structures, symmetry reduction of the ball yields spectra of increasing complexity, partly manifest in splitting of modes derived from the degenerate T_{1u} and H_g vibrations of I_hC_{60}.[3,4,14,16,22–26] Mode splittings of the rhombohedral HPHT polymer and linear chain RbC_{60} were initially treated by group theory analysis, based on a weak perturbation assumption.[24] Later work found, however, that the weak perturbation picture is inadequate to explain certain widely split or shifted modes in the HPHT polymers and dimer.[27] A realistic prediction of the vibrational spectrum of such structures requires a theoretical calculation that takes into account significant distortion of the C_{60} balls due to intermolecular bonding. Calculated vibrational spectra for the linear chain polymer and different dimer structures[28–32] have been used to identify the 2+2 cycloaddition dimer in some phototransformed C_{60} materials.[26,28,30–32] Such treatments usually have focused on the Raman spectra, for which calculated mode strengths are more reliable,[28,33] and which exhibit low-frequency features characteristic of intermolecular vibrations.[3,14,15,34,35]

In this paper, we report far-infrared (FIR) vibrational properties of the 2+2 cycloaddition dimer, and the 1D orthorhombic and 2D rhombohedral HPHT C_{60} polymers whose structures are shown in Fig. 1. Hereafter, we refer to these structures as the dimer, the *O* polymer, and the *R* polymer, respectively. We combine high-resolution FIR transmittance measurements with first-principles quantum molecular-dynamics calculations in order to investigate intermolecular bonding and symmetry breaking in this class of fullerene-derived materials. We focus on the FIR frequency region, 20–650 cm^{-1}, which allows us to search for intermolecular modes below 200 cm^{-1} and identify features derived from I_hC_{60} modes in the lower frequency portion of the intramolecular spectrum (below 400 cm^{-1}), which has not been measured in previous IR studies of these systems.[3,4,16,17,22–26,36] Using detailed assignments of on-ball vibrations, we confirm both very narrow and unprecedentedly wide mode splittings which characterize the vibrational spectra of the three different structures.

II. MATERIALS AND METHODS

Samples of the 2+2 cycloaddition C_{60} dimer were made by pressing the compound $(ET)_2C_{60}$ [ET =bis(ethylenedithio)tetrathiafulvalene] to 5 GPa at 200°C, after which the ET was removed by sonication in CH_2Cl_2.[17] For the orthorhombic polymer, C_{60} powder was wrapped in tantalum foil and pressed for 1 h at 1.5 GPa and 300 °C inside a lava mold using a piston/cylinder-type press. X-ray diffraction confirmed the same orthorhombic structure as reported in Ref. 10, with an estimated domain size of 15–20 nm.[37] The rhombohedral polymer samples were synthesized at 5 GPa and 700 °C as described in Ref. 4. The rhombohedral structure was confirmed by x-ray diffraction, which indicated 18–23-nm crystalline domain size.[38] All materials were crushed into powder, ground with paraffin at 77 K, and compressed under vacuum at 1.5 kbar to form isotropic pellets suitable for FIR transmittance studies.[39] Concentrations were optimized for different frequency regimes.

We made far-infrared transmittance measurements on a Bruker 113V FTIR spectrometer. A series of four different beam splitters covered the spectral region 20–650 cm^{-1}. A Si bolometer detector, cooled to 4 K, provided extra sensitivity. Repeated measurements of the low-temperature spectra ($T\approx 20$ K), obtained with an open flow cryostat system, yielded good reproducibility of features, although some very weak peaks were found only in the most concentrated samples. We determined vibrational mode frequencies from the low T spectra, which were made using 0.5 or 1.0 cm^{-1} resolution, depending on the frequency range. Only minor splitting and hardening (on the order of 1 cm^{-1}) of transmission peaks were observed at 20 K compared to 300 K, with the exception of a weak feature near 240 cm^{-1}, which does not appear in the room-temperature spectra. Where interference fringes obscured some low-energy fine structure, we subtracted a fit to the fringes, which consisted of a damped sine curve plus a linear background.[40] In some cases, fringes were reduced by smoothing.

For calculating the equilibrium geometries, normal modes, and first-order (fundamental) IR strengths, we have used quantum molecular dynamics (QMD), a first-principles technique initiated by Sankey and Niklewski.[41] A first-principles calculation allows one to obtain the equilibrium geometry and the vibrational properties without fitting parameters. The Born-Oppenheimer (adiabatic) approximation is utilized throughout the calculation, and the normal modes and IR strengths are calculated in the harmonic and linear electric dipole moment approximations. In QMD, the adiabatic many-electron ground-state wave function is expanded in a basis of real-space confined pseudoatomic orbitals of *s* and *p* types, centered on each carbon atom. For each MD time step, this wave function, the electronic eigenvalues, and the atomic forces are computed within the local-density approximation (LDA) and the Harris-energy-functional approximation. The forces are used in QMD simulations, with damping added, to yield the relaxed equilibrium geometries. Then, by computing atomic forces per unit displacement of individual atoms from the equilibrium geometry, the harmonic force constants are obtained, yielding the normal modes. The method has been applied successfully to fullerene molecules,[42] polymerized fullerenes,[28,43] and to novel carbon solids.[44] For the *O*- and *R*-polymer calculations in this work, we have used one C_{60} ball per periodic unit cell,[45,46] so that all mode displacement patterns are identical on each ball, i.e., all modes are of zero wave vector in a one-ball-per-cell description.

TABLE I. Symmetry analysis of intramolecular modes in the dimer, orthorhombic, and rhombohedral geometries.

I_h	2+2 cycloaddition dimer ($C_{2v}\rightarrow D_{2h}$)	Orthorhombic (D_{2h})	Rhombohedral (D_{3d})
$2A_g$	$2A_g+2B_{1u}$	$2A_g$	$2A_{1g}$
$3T_{1g}$	$3B_{1g}+3B_{2g}+3B_{3g}+3A_u+3B_{2u}+3B_{3u}$	$3B_{1g}+3B_{2g}+3B_{3g}$	$3A_{2g}+3E_g$
$4T_{3g}$	$4B_{1g}+4B_{2g}+4B_{3g}+4A_u+4B_{2u}+4B_{3u}$	$4B_{1g}+4B_{2g}+4B_{3g}$	$4A_{2g}+4E_g$
$6G_g$	$6A_g+6B_{1g}+6B_{2g}+6B_{3g}+6A_u+6B_{1u}+6B_{2u}+6B_{3u}$	$6A_g+6B_{1g}+6B_{2g}+6B_{3g}$	$6A_{1g}+6A_{2g}+6E_g$
$8H_g$	$16A_g+8B_{1g}+8B_{2g}+8B_{3g}+8A_u+16B_{1u}+8B_{2u}+8B_{3u}$	$16A_g+8B_{1g}+8B_{2g}+8B_{3g}$	$8A_{1g}+16E_g$
$1A_u$	$1B_{1g}+1A_u$	$1A_u$	$1A_{1u}$
$4T_{1u}$	$4A_g+4B_{2g}+4B_{3g}+4B_{1u}+4B_{2u}+4B_{3u}$	$4B_{1u}+4B_{2u}+4B_{3u}$	$4A_{2u}+4E_u$
$5T_{3u}$	$5A_g+5B_{2g}+5B_{3g}+5B_{1u}+5B_{2u}+5B_{3u}$	$5B_{1u}+5B_{2u}+5B_{3u}$	$5A_{2u}+5E_u$
$6G_u$	$6A_g+6B_{1g}+6B_{2g}+6B_{3g}+6A_u+6B_{1u}+6B_{2u}+6B_{3u}$	$6A_u+6B_{1u}+6B_{2u}+6B_{3u}$	$6A_{1u}+6A_{2u}+6E_u$
$7H_u$	$7A_g+14B_{1g}+7B_{2g}+7B_{3g}+14A_u+7B_{1u}+7B_{2u}+7B_{3u}$	$14A_u+7B_{1u}+7B_{2u}+7B_{3u}$	$7A_{1u}+14E_u$
Total Raman:			
$10(A_g,H_g)$	$174(A_g,B_{1g},B_{2g},B_{3g})$	$87(A_g,B_{1g},B_{2g},B_{3g})$	$45(A_{1g},E_g)$
Total IR:			
$4(T_{1u})$	$132(B_{1u},B_{2u},B_{3u})$	$66(B_{1u},B_{2u},B_{3u})$	$44(A_{2u},E_u)$

Knowledge of the many-electron ground-state wave function for a given atomic configuration allows one to compute directly the total electric dipole moment for that configuration. Including just terms linear in the atoms' displacements yields the atoms' IR effective charges. These are combined with the normal mode displacement patterns to give the mode dipole moments, the squares of which give the areas under the modes' IR lines. Although the predicted spectrum consists of temperature-independent δ-function lines at each IR frequency, in practice these are given Lorentzian broadening. Additional details of our methods for computing the equilibrium geometries, normal modes, and IR strengths are given in the references cited in the preceding paragraph and in recent reviews.[32,33]

III. GROUP-THEORY PREDICTIONS AND MOLECULAR-DYNAMICS CALCULATIONS

For the case of a weakly distorted molecule, a group-theory correlation method may be used to predict splittings and activations of vibrational modes produced by the molecular symmetry reduction. Since a small distortion will manifest itself in fine multiplet splittings or minor energy shifts, modes of the perturbed molecule can be correlated with modes of the higher symmetry molecule. This weak perturbation approach has been successfully applied to $(Ph_4P)_2IC_{60}$, in which the isolated singly charged ball undergoes a Jahn-Teller distortion and the I_hC_{60} vibrations become narrowly split.[40] On the other hand, this type of model cannot adequately describe the vibrational properties of a strongly distorted ball (as in the bonded structures of interest here), which may exhibit wide splittings, large energy shifts, and mode mixing. Nevertheless, a review of the group theory will provide a useful introduction to the expected changes in numbers of mode activations and splittings, although it provides no information on the energetics. Note, in addition, that group theory selection rules cannot say which allowed modes will have sufficient intensity to be observed.

Table I shows the expected splittings of modes upon symmetry reduction from the original I_h symmetry of the C_{60} cage. For the dimer, we used the correlation method[47] with site symmetry C_{2v} and dimer molecule symmetry D_{2h}, taking the z axis as the intradimer bond direction.[48] The derivation for the orthorhombic and rhombohedral structures is straightforward, since the respective point groups, D_{2h} and D_{3d}, are subgroups of I_h. Selection rules determine which modes can be infrared or Raman active as well as the multiplicity of I_h-derived modes in each reduced-symmetry point group. For example, the T_{1u}-derived modes are split into doublets (with some remaining degeneracy) in the D_{3d} point group and into nondegenerate triplets in D_{2h}. Since the presence of inversion symmetry renders the infrared and Raman modes mutually exclusive, only odd vibrations and no even (Raman-active) ones should be observed in the IR spectra of the R and O polymers. Only in the dimer, where individual balls have lost their inversion symmetry, do we expect to see infrared-active modes derived from even (g) modes of I_hC_{60}. Thus, the dimer spectrum is expected to be the most complex, because it contains the most allowed modes, and the R-polymer spectrum the simplest.

Figure 2 displays our first-principles predicted IR spectra for I_hC_{60}, the dimer, the O polymer, and the R polymer. The 480–620-cm^{-1} region is chosen because it contains the $T_{1u}(1)$ and $T_{1u}(2)$ vibrations or modes derived from them. The frequencies we calculate for $T_{1u}(1)$ and $T_{1u}(2)$ in I_hC_{60} (522 and 570 cm^{-1}) are in excellent agreement with the experimental values (526 and 575 cm^{-1}). Similar agreement is found for the eleven non-IR-active C_{60} modes in the region 300–700 cm^{-1},[32] giving us confidence in our calculated frequencies in this range. Although we find good reliability in our calculated frequencies, the calculated intensities contain a large degree of uncertainty, as detailed in Sec.

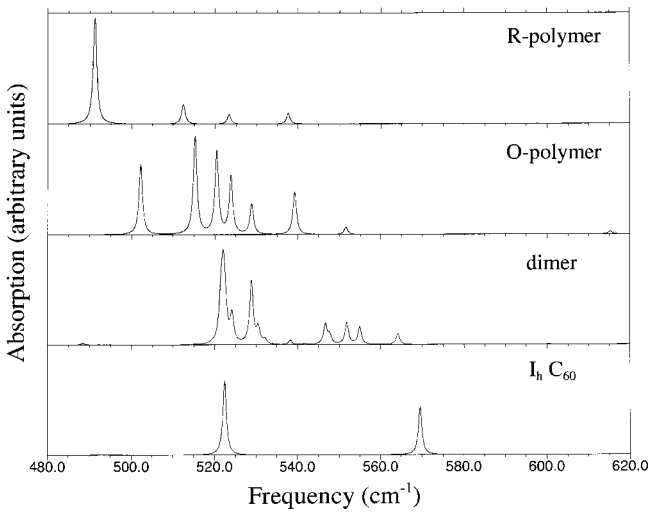

FIG. 2. Calculated IR spectra for I_hC_{60}, the dimer, the *O* polymer, and the *R* polymer, in the 480–620-cm^{-1} region. The IR peaks have been broadened into Lorentzians of width 1 cm^{-1} (FWHM). As discussed in the text, we have not used the calculated strengths in making our assignments.

2.3 of Ref. 32. Specifically, the predicted relative strengths, normalized to that of $T_{1u}(1)$, are (1.0: 0.65: 1.4: 0.31), whereas the experimental values[49] are (1.0: 0.34: 0.28: 0.34). Thus, while our strengths for $T_{1u}(2)$ and $T_{1u}(4)$ are in qualitative agreement with experiment, that for $T_{1u}(3)$ is a factor of five too large. Accordingly, the calculated IR strengths cannot be used to identify the IR peaks unambiguously, and we therefore make assignments using the calculated frequencies only. On the scale of Fig. 2, several modes with weak calculated intensities disappear from the spectrum, but are used to assign observed features in the FIR data, based on similar frequencies.

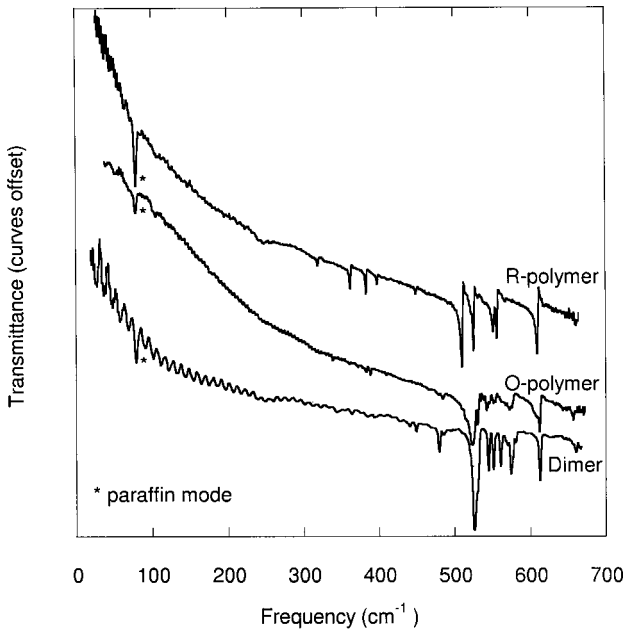

FIG. 3. The complete experimental FIR spectra of low-temperature transmittance versus frequency for the *R* polymer, *O* polymer, and dimer. The curves are offset for clarity; the mode marked by an asterisk is due to paraffin.

As is evident in Fig. 2, we predict significant softening (downshift) of the T_{1u} vibrations in the *R*-polymer compared to I_hC_{60}, and less softening for modes of the *O*-polymer and dimer structures, which contain fewer interball connections. The softening results from a loss of double bonds on the cage due to the formation of bonds between balls, as previously noted by Rao *et al.*[22] As will be discussed in detail for the individual bonded structures, the calculated spectra also exhibit wide splittings of modes. Most notable are instances where the $T_{1u}(2)$-derived vibration, polarized along the stretched (bonding) direction, is downshifted below all $T_{1u}(1)$-derived modes. The overlap of $T_{1u}(2)$- and $T_{1u}(1)$-derived modes is most pronounced for the *R*-polymer, which has the most distorted C_{60} balls, and does not occur in the dimer, which has the least perturbed balls. Despite uncertainty in the mode strengths, the calculated spectra follow a trend of increasing complexity in the sequence *R* polymer : *O* polymer : dimer, consistent with the increasing number of symmetry-allowed modes (Table I).

IV. RESULTS AND DISCUSSION

A. Comparison of overall FIR spectra

Figure 3 shows the low-temperature FIR transmission spectra of the *R* polymer, the *O* polymer, and the dimer. All three materials exhibit a rich vibrational spectrum in the intramolecular region, in accord with the reduced symmetry of the ball. Strong vibrational structure is particularly concentrated in the 500–600 cm^{-1} region, implying that in the bonded structures the $T_{1u}(1)$ and $T_{1u}(2)$ modes of I_hC_{60} have split and new modes have been activated. Newly-activated modes also appear between 300 and 500 cm^{-1} and above 600 cm^{-1}. In the region below 200 cm^{-1}, no vibrational features are observed save for the 80-cm^{-1} mode of paraffin. For the *O* and *R* polymers, inter-ball modes in the perfect crystals cannot be IR-active, so any observed IR-activity in this range would be due to the effects of finite domain size or other symmetry breaking. If such IR-active vibrations exist for the *O* and *R* polymers, they occur at frequencies below our range or are simply too weak to be detected. Interball vibrations have been observed in Raman spectra of the dimer,[14] photopolymer,[3,50] and HPHT polymers[12,34] in good agreement with calculated frequencies[28,30] and by inelastic neutron scattering in the *O* polymer.[51] Although IR-active interball modes are predicted near 22 and 35 cm^{-1} in the dimer,[30,31] we do not resolve them here. In the following, we focus on the symmetry breaking of on-ball modes, observed above 200 cm^{-1}.

Detailed comparison of the FIR transmittance and calculated frequencies allows us to identify most of the vibrational features in each bonded structure. Experimental and theoretical mode frequencies are given in Tables II, III, and IV, for the *R* polymer, dimer, and *O* polymer, respectively. The percent errors between the experimental (ν_e) and theoretical (ν_t) frequencies, defined as $100\times(\nu_t-\nu_e)/\nu_e$, are listed in the final column of each table. Consistent with our previous results,[32] we find that the calculated frequencies in the FIR region are generally a few percent low and that a positive error is quite unusual. The tables also list the degeneracy, symmetry, ''parent symmetry,'' and polarization of the calculated modes. ''Parent symmetry'' refers to the symmetry

TABLE II. Experimental and calculated IR modes of the rhombohedral polymer. The site symmetry is D_{3d}, and the IR-active modes are twofold degenerate (E_u) or nondegenerate (A_{2u}). ''Parent symmetry'' refers to the symmetry of the $I_h C_{60}$ mode from which the *R*-polymer vibration is found to be derived. A ''$\sim$'' indicates that identification of the parent symmetry for that mode is not unambiguous. Four-connected balls are discussed in Sec. IV B.

Experimental frequency (cm^{-1})	Calculated frequency (cm^{-1})	Degeneracy	Symmetry	Parent symmetry	Polarization	Error (%)
247						
319	299	2	E_u	$\sim T_{3u}(1)$	in-plane	−6.3
	320	2	E_u	$\sim G_u(1)$	in-plane	
362	336	1	A_{2u}	$\sim T_{3u}(1)$	normal-to-plane	−7.2
383	366	2	E_u	$\sim H_u(1)$	in-plane	−4.4
398	401	2	E_u	$\sim H_u(1)$	in-plane	+0.75
450	429	1	A_{2u}	$\sim G_u(1)$	normal-to-plane	−4.7
510	491	2	E_u	$T_{1u}(2)$	in-plane	−3.7
515	496	1	A_u	four-connected ball, $T_{1u}(2)$		−3.7
522	508	1	A_u	four-connected ball		−2.7
525	512	2	E_u	$\sim T_{1u}(1)$	in-plane	−2.5
531	523	1	A_{2u}	$T_{1u}(1)$	normal-to-plane	−3.5
538	530	1	A_u	four-connected ball		−1.5
552	534	2	E_u	$\sim H_u(2)$	in-plane	−3.3
557	538	1	A_{2u}	$T_{1u}(2)$	normal-to-plane	−3.4
567	555	1	A_u	four-connected ball		−2.1
610	598	2	E_u	$\sim H_u(2)$	in-plane	−2.0

of the $I_h C_{60}$ mode from which the reduced-symmetry ball vibration is found to be derived. To determine the parent symmetry of calculated modes, we made a visual comparison of the mode displacement patterns in the polymerized structures to those in $I_h C_{60}$. For all three polymerized structures, the $T_{1u}(2)$-derived modes can be confidently identified, as is demonstrated in Fig. 4. In most cases, however, whereas the mode patterns of the polymerized structures are found to have characteristics of an $I_h C_{60}$ mode, the visual agreement is not unambiguous. Such cases are indicated by ''$\sim$'' in Tables II, III, and IV.

Figures 5, 6, and 7 display closeups of the low-temperature vibrational spectra, divided into $\approx$100-cm^{-1} regions that reflect natural divisions of the $I_h C_{60}$ vibrations: the 200–300-cm^{-1} region contains only the Raman-active $H_g(1)$ mode, the 300–400-cm^{-1} region contains three silent odd modes, the 400–500-cm^{-1} region contains only even modes, and the 500–620-cm^{-1} region contains $T_{1u}(1)$ and $T_{1u}(2)$ and both odd and even silent vibrations. We begin our discussion of the different bonded structures with the *R* polymer, which has the simplest spectrum of the three (in good accord with the group-theory analysis) and the easiest to interpret. We then move on to the dimer, where we also have good success, and save for last the *O* polymer, which unexpectedly has the most complex spectrum, and where a number of questions remain.

B. Rhombohedral polymer

Table II lists the vibrational frequencies between 200 and 630 cm^{-1}, obtained from the QMD calculations for the C_{60} ball in a rhombohedral structure. The major result is that $T_{1u}(2)$ is substantially split (by 47 cm^{-1}) and its lower frequency component (polarized in the stretched direction, as shown in Fig. 4) is downshifted below both $T_{1u}(1)$-derived modes. This result implies immediately that a small perturbation picture is inadequate in this material. Despite the fact that only $T_{1u}(2)$-derived modes could be unambiguously identified from mode displacement patterns (due to the orientation and distortion of the C_{60} ball), the known double degeneracy of IR-active H_u-derived modes[24] allows us to positively identify the singly degenerate 523-cm^{-1} mode as derived from $T_{1u}(1)$. Other tentative parent symmetry identifications suggest additional wide mode splittings, including $H_u(2)$ split by 64 cm^{-1} and $G_u(1)$ split by 109 cm^{-1}. In contrast, $T_{1u}(1)$ is split by only 11 cm^{-1}.

In Table II some of the weaker *R* polymer features are assigned as ''four-connected ball'' modes. A four-connected ball structure is the most likely bonding configuration along the edges of rhombohedral domains. These edges can be visualized by mentally removing the leftmost or rightmost column of C_{60} balls (and bonds to them) in Fig. 1(c); the individual four-connected ball structure is shown in Fig. 4(e). We have calculated the IR spectrum of these four-connected balls,[52] although it is not shown here. Since such balls will be in the minority unless the domains are very small, only the strongest four-connected ball modes, which are likely to be T_{1u}-derived, should appear in the *R* polymer spectrum. The four-connected ball vibrations also include *g*-derived modes, due to the lack of inversion symmetry. C_{60} balls with other polymer connectivities will also be present, due to a variety of defects at the edges and interiors of the rhombohedral domains, but these will have an even weaker contribution to the spectrum.

TABLE III. Experimental and calculated modes of the dimer. The symmetry of the dimer is D_{2h}. All modes are nondegenerate. ''Parent symmetry'' refers to the symmetry of the $I_h C_{60}$ mode from which the dimer vibration is found to be derived. A ''$\sim$'' indicates that identification of the parent symmetry for that mode is not unambiguous. For the polarizations: z is the dimer axis, y is normal to the plane of the four-membered ring connecting the balls, and x is in that plane and normal to z.

Experimental frequency (cm^{-1})	Calculated frequency (cm^{-1})	Symmetry	Parent symmetry	Polarization	Error (%)
241	243	B_{1u}	$H_g(1)$	z	+0.8
250	252	B_{1u}	$H_g(1)$	z	+0.8
254	256	B_{3u}	$H_g(1)$	x	+0.8
260	256	B_{2u}	$H_g(1)$	y	−1.5
343	321	B_{1u}	$\sim T_{3u}(1)$	z	−6.4
345	330	B_{2u}	$\sim T_{3u}(1)$	y	−4.3
349	334	B_{3u}	$\sim T_{3u}(1)$	x	−4.3
	345	B_{1u}	$\sim G_u(1)$	z	
	346	B_{3u}	$\sim G_u(1)$	x	
363	348	B_{2u}	$\sim G_u(1)$	y	−4.1
384	386	B_{2u}	$\sim H_u(1)$	y	+0.5
	388	B_{1u}	$\sim H_u(1)$	z	
394	391	B_{3u}	$\sim H_u(1)$	x	−0.8
	417	B_{1u}	$\sim H_g(2)$	z	
428	421	B_{2u}	$\sim H_g(2)$	y	−1.6
441	430	B_{1u}	$\sim H_g(2)$	z	−2.5
450	435	B_{3u}	$\sim H_g(2)$	x	−3.3
479					
	460	B_{1u}	$A_g(1)$	z	
480	469	B_{3u}	$\sim G_g(1)$	x	−2.3
485					
486	475	B_{2u}	$\sim G_g(1)$	y	−2.1
496	488	B_{1u}	$\sim G_g(1)$	z	−0.4
525	521	B_{2u}	$\sim T_{1u}(1)$	y	−0.8
526	522	B_{1u}	$\sim T_{1u}(1)$	z	−0.8
526	522	B_{3u}	$\sim T_{1u}(1)$	x	−0.8
527	524	B_{2u}	$\sim H_u(2)$	y	−0.6
530	529	B_{3u}	$\sim H_u(2)$	x	−0.2
531	530	B_{1u}	$T_{1u}(2)$	z	−0.2
532	532	B_{2u}	$\sim T_{3g}(1)$	y	0.0
545	538	B_{3u}	$\sim T_{3g}(1)$	x	−1.3
551	546	B_{1u}	$\sim H_u(2)$	z	−0.9
555					
561	552	B_{2u}	$T_{1u}(2)$	y	−1.6
562	542	B_{1u}	$\sim G_g(2)$	z	−3.5
567					
568					
570	548	B_{3u}	$\sim G_g(2)$	x	−3.8
574	555	B_{2u}	$\sim G_g(2)$	y	−3.3
577	564	B_{3u}	$T_{1u}(2)$	x	−2.2
581	572	B_{2u}	$\sim T_{1g}(1)$	y	−1.5
612	600	B_{3u}	$\sim T_{1g}(1)$	x	−2.0
613					

Some calculated frequencies are out of order to preserve the listed order of experimental frequencies.

Figure 5 shows a detailed view of the FIR spectrum of the *R* polymer, with frequencies labeled for all reproducible peaks, some of which are quite weak. There is a broad but weak feature near 247 cm^{-1}, which must originate in $H_g(1)$ and is discussed below in conjunction with other evidence of reduced-symmetry balls. Five newly activated modes appear between 300 and 500 cm^{-1}, most of which are very intense. These are easily assigned to five of the six calculated modes

TABLE IV. Experimental and calculated modes of the orthorhombic polymer. The site symmetry is D_{2h}. All modes are nondegenerate. ''Parent symmetry'' refers to the symmetry of the $I_h C_{60}$ mode from which the *O*-polymer vibration is found to be derived. A ''$\sim$'' indicates that identification of the parent symmetry for that mode is not unambiguous. For the polarizations: *z* is in the chain direction; *y* is normal to the plane of the four-membered rings connecting the balls; and *x* is in that plane and normal to *z*.

Experimental frequency (cm^{-1})	Calculated frequency (cm^{-1})	Symmetry	Parent symmetry	Polarization	Error (%)
244					
	308	B_{1u}	$T_{3u}(1)$	z	
	321	B_{3u}	$G_u(1)$	x	
339	327	B_{2u}	$T_{3u}(1)$	y	-3.5
	349	B_{1u}	$G_u(1)$	z	
360	352	B_{2u}	$G_u(1)$	y	-2.2
372	366	B_{3u}	$T_{3u}(1)$	x	-1.6
383	379	B_{1u}	$H_u(1)$	z	-1.0
389	380	B_{2u}	$H_u(1)$	y	-2.3
410	398	B_{3u}	$H_u(1)$	x	-2.9
515	502	B_{1u}	$T_{1u}(2)$	z	-2.5
520	515	B_{3u}	$T_{1u}(1)$	x	-1.0
524	520	B_{1u}	$T_{1u}(1)$	z	-0.8
527	516	B_{2u}	$\sim H_u(2)$	y	-2.1
531	524	B_{2u}	$\sim T_{1u}(1)$	y	-1.3
543	529	B_{2u}	$T_{1u}(2)$	x	-2.6
554	539	B_{2u}	$T_{1u}(2)$	y	-2.7
572	552	B_{1u}	$H_u(2)$	z	-3.5
613	593	B_{3u}	$H_u(2)$	x	-3.2
	615	B_{3u}	$H_u(3)$	x	

Some calculated frequencies are out of order to preserve the listed order of experimental frequencies.

in this region (see Table II), yielding the expected doublets for two of the three newly allowed odd modes. Most notably, the presence of a sharp feature at 450 cm^{-1} [upshifted almost 100 cm^{-1} from the silent $G_u(1)$ mode at 353 cm^{-1} in $I_h C_{60}$] supports our prediction of an extraordinarily large splitting of $G_u(1)$. Note that there is some ambiguity in the identification of the 319 cm^{-1} feature, due to two candidates for its assignment. The general agreement between experimental and calculated frequencies in this region is quite good, with errors between $+1$ and -7%.

In the 500–620-cm^{-1} region of the *R* polymer spectrum, we observe several intense peaks, in good agreement with published results,[24] as well as some weaker features that were previously undetected. Based on the calculated frequencies and mode patterns, we assign a wide doublet splitting of $T_{1u}(2)$ and narrow splitting of $T_{1u}(1)$ (see Table II). Interestingly, the latter is divided into strong and weak components, at 525 and 531 cm^{-1}, respectively, whereas both halves of the $T_{1u}(2)$ doublet remain strong. The $H_u(2)$ mode of $I_h C_{60}$ appears to be strongly activated in this polymer, with the high-frequency component at 610 cm^{-1} providing further evidence of the wide splittings that occur in the *R* polymer. Indeed, the assignment of the 610-cm^{-1} mode exemplifies the success of the QMD calculations and supports the picture of a strongly distorted ball. This feature was previously unassigned in a weak perturbation picture,[24,27] due to the absence of nearby silent modes in the $I_h C_{60}$ spectrum.[32,53] Overall, the agreement between experimental and calculated frequencies for the rhombohedral modes between 500 and 620 cm^{-1} is good, with errors between -2 and -4.4%.

The weaker *R* polymer features appearing between 500 and 600 cm^{-1} are explained well by the vibrational spectrum of four-connected balls, which we have calculated, as noted above. Three of the modes labeled ''four-connected ball'' in Table II are the strongest of the calculated four-connected ball spectrum. One of these modes is identifiable as $T_{1u}(2)$-derived [see Fig. 4(e)], and the other two, being strong, probably derive from T_{1u} vibrations as well. A weak *R* polymer mode at 567 cm^{-1} may also be due to the four-connected balls or might be the combination mode of $H_g(1) \otimes T_{3u}(1)$, which could appear at 566 cm^{-1}. By extracting the relative intensities of four-connected ball and rhombohedral modes from the FIR data, we estimate a ratio of edge balls to interior balls between 1:7 and 1:10. This estimate implies a domain diameter of approximately 28–40 nm, which is in relatively good agreement with the 18–23-nm value obtained by x-ray diffraction,[38] assuming an underestimate of the domain size due to other broadening effects on the diffraction peaks. A diminished effect of four-connected balls and a concomitant overestimate of domain size from the FIR data could be due as well to the presence of defects along the domain edges. The calculated four-connected ball spectrum also contains a weak quadruplet of $H_g(1)$-derived modes, of which either the 237 or 244 cm^{-1} vibration might explain the broad weak feature at 247 cm^{-1} in the *R* polymer.

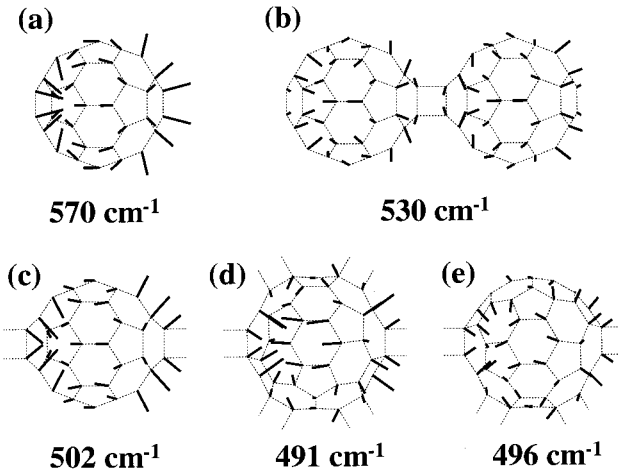

FIG. 4. Vibrational mode displacement patterns. (a) A selected $T_{1u}(2)$ mode of $I_h C_{60}$. (b)–(e) The $T_{1u}(2)$-derived mode which is polarized in the bonding direction of (b) the dimer, (c) the *O* polymer, (d) the *R* polymer, and (e) the four-connected balls which are the most probable structures at the edges of *R* polymer domains. All figures are drawn to scale. Note that the static equilibrium configurations of the C_{60} balls in the polymers are stretched in the bonding directions. The stretching is greatest for the balls in the *R* polymer, where the width of the balls in the bonding directions is 11% longer than the corresponding width in $I_h C_{60}$.

C. Dimer

In the dimer the calculated vibrational splittings and frequency shifts due to bonding are small compared to those in the polymers because of fewer interball connections and less distortion of the C_{60} balls. The calculated frequencies are

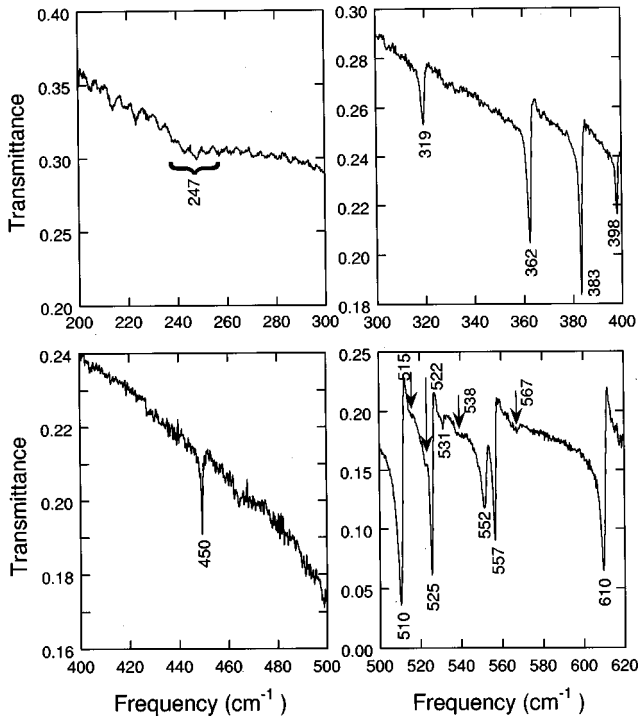

FIG. 5. Close-up plots of each $\approx$100-cm^{-1} region of the low-temperature transmittance versus frequency for the *R* polymer. Frequencies are labeled for all reproducible modes.

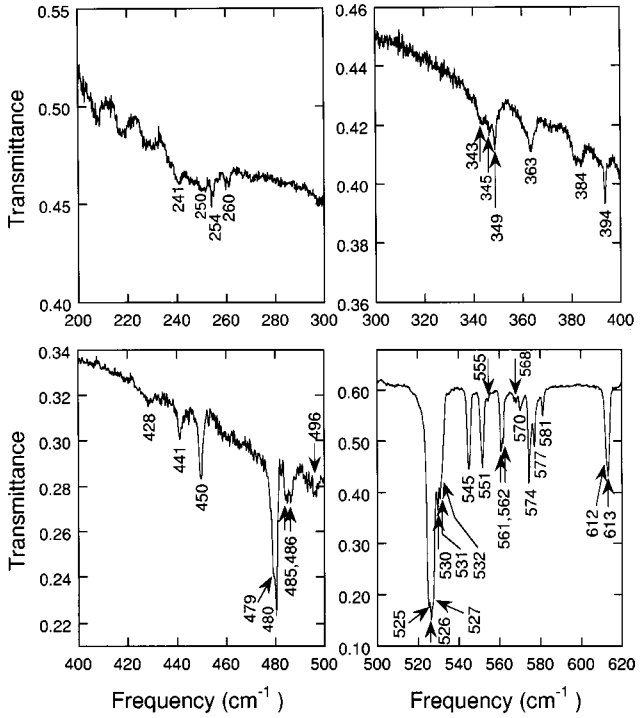

FIG. 6. Close-up plots of each $\approx$100-cm^{-1} region of the low-temperature transmittance versus frequency for the dimer. Frequencies are labeled for all reproducible modes. Different concentrations of dimer in the paraffin matrix account for different transmission levels in the different regions.

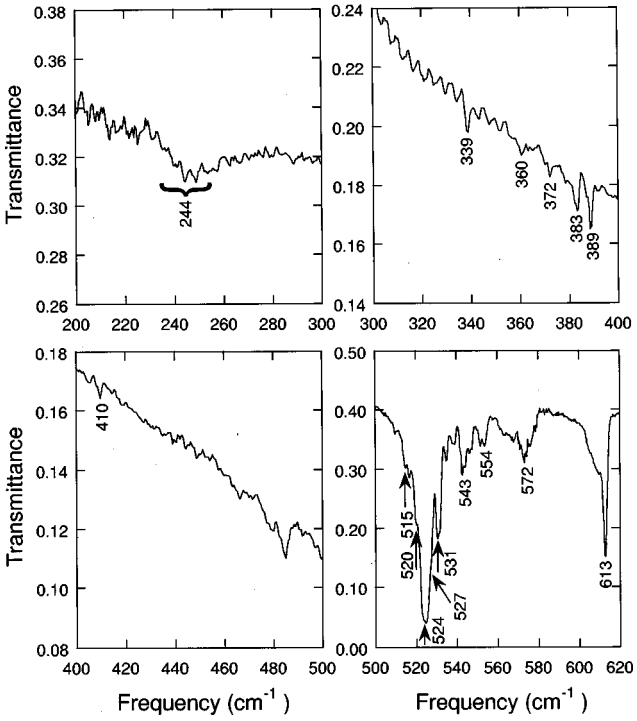

FIG. 7. Close-up plots of each $\approx$100-cm^{-1} region of the low-temperature transmittance versus frequency for the *O* polymer. Frequencies are labeled only for those modes for which we make tentative assignments. Other reproducible features of the *O*-polymer spectrum are listed in Ref. 53. Different concentrations of *O* polymer in the paraffin matrix account for different transmission levels in the different regions.

listed in Table III. As mentioned in Sec. III, the density of IR-active modes is much greater than for the *R* or *O* polymers because the lack of inversion symmetry in each ball of the dimer allows odd dimer modes to be derived from even modes of I_hC_{60}, with the two balls vibrating out of phase. The mode pattern analysis is complicated by this lack of inversion symmetry in the individual balls. Only $H_g(1)$-, $A_g(1)$-, and $T_{1u}(2)$-derived modes could be unambiguously identified by mode displacement patterns. As for the *R* polymer, some frequency overlapping occurs for the component of the $T_{1u}(2)$-derived mode polarized in the bonding direction, but it downshifts only below $H_u(2)$-*z*, and not below the $T_{1u}(1)$-derived modes. Compared to the substantial splitting of $T_{1u}(2)$, other modes are narrowly split [$T_{1u}(1)$ splits by just 1 cm^{-1}] and bunched together in groups. Note that we calculated an extremely weak intensity of the $A_g(1)$-derived mode, which is probably reliable due to the high symmetry of this mode, so we do not expect to see it in the FIR data and do not assign it in Table III. Overall, the calculated spectrum is very rich, including multiplets of modes activated from both odd and even silent vibrations of I_hC_{60}.

Figure 6 displays our FIR transmittance results for the dimer, with frequencies labeled for the reproducible peaks. In general, the frequencies and appearance of the spectrum are in reasonable agreement with previously published results for the purified mechanochemically-reacted dimer, with some inconsistencies likely attributable to the lower resolution of the measurements of Ref. 25. $H_g(1)$-derived modes are allowed in the dimer and appear as a weak quadruplet near 250 cm^{-1}, very close to the calculated frequencies. Odd modes of I_hC_{60} between 300 and 400 cm^{-1} are not as strongly activated in the dimer as in the *R* polymer. The $T_{3u}(1)$-derived modes are found to be three in number, in agreement with group-theory predictions for the D_{2h} symmetry of the dimer. In the 400–500-cm^{-1} region, we observe some strongly active $H_g(2)$- and $G_g(1)$-derived vibrations, which can be odd and IR active in the dimer, as mentioned above. Assuming our neglect of the weak $A_g(1)$-derived mode is correct, we observe two more FIR features than expected between 460 and 500 cm^{-1}. These two peaks may originate in combinations (two phonon processes) of odd and even H_g-derived vibrations, or in some other mechanism which causes fine splitting of the 480- and 486-cm^{-1} $G_g(1)$-derived vibrations.

Between 500 and 620 cm^{-1}, the dimer exhibits a high density of modes, including several closely grouped vibrations and fine splittings that are in qualitative agreement with the calculated spectrum. Some of the T_{3g}-, $G_g(2)$-, and T_{1g}-derived modes are found to be strongly active. In making assignments within this region, we attempted to preserve the calculated frequency ordering that results from mode-pattern analysis, as well as the relative splittings within each doublet or triplet. Of the various assignment permutations we tried, none preserved the order while simultaneously matching the expected groupings, so our best assignments are a compromise and should be taken only as the most probable case. (The experimental mode frequencies are listed in sequential order in Table III, which makes some calculated frequencies out of order.) Note that $T_{1u}(1)$-derived components are barely downshifted from the I_hC_{60} $T_{1u}(1)$ frequency, in excellent agreement with the ≤ 1 cm^{-1} predicted downshifts. In general, calculated and experimental frequencies are in good accord in this region, with errors ranging between 0.0 and -3.8%, and an average of -1.4%. Note, however, that this low average error is in part an artifact of the high density of modes and may not reflect accurate assignments of individual modes.

One of the successes of our dimer assignments is an identification of the intense mode at 612 cm^{-1}, which cannot be assigned in a weak perturbation picture.[27] Note that the $T_{1g}(1)$ assignment of this mode is different from the $H_u(2)$ assignment of the 610-cm^{-1} mode in the *R* polymer, and is consistent with the different shape of this feature in the dimer. In the calculated spectrum, $T_{1g}(1)$ is split and shifted to higher energy (600 cm^{-1}) from its location at 568 cm^{-1} in I_hC_{60}. The strong calculated shift explains the appearance of the 612 cm^{-1} feature in our data, where none would be expected in a weak perturbation model, due to the lack of nearby I_hC_{60} modes.[32,53] The observed fine doublet splitting of the 612 cm^{-1} feature is unaccounted for in the calculated spectrum, however. One possible origin of the splitting is the effect of crystal packing and interdimer interactions, which could similarly account for the aforementioned splitting of $G_g(1)$-derived modes. Table III lists a few peaks of the dimer that remain unassigned by the calculations. Most of these are very weak spectral features at frequencies which could be combination modes.[54]

D. Orthorhombic polymer

The calculated spectrum of the *O* polymer (frequencies listed in Table IV) contains large splittings similar to those of the *R* polymer, although downshifts from the I_hC_{60} modes are smaller, as previously noted. Symmetry identification by mode pattern is straightforward except for modes $H_u(2)$-*y* and $T_{1u}(1)$-*y* which appear to mix. In particular, $T_{1u}(2)$ is widely split and the component along the chain direction is again downshifted below any $T_{1u}(1)$-derived mode, whereas $T_{1u}(1)$ is very narrowly split. $T_{3u}(1)$ and $H_u(2)$ are widely split. Note that in the *O* polymer, all odd modes divide into triplets due to the D_{2h} point group of the ball, in contrast to doublets in the *R* polymer due to the D_{3d} symmetry.

Figure 7 displays the detailed FIR spectrum of the *O* polymer, with frequencies labeled for only those features that we attempt to assign. Weak reproducible features are found in the regions 200–300 cm^{-1} and 400–500 cm^{-1}. Since these ranges contain only even vibrations for I_hC_{60}, we attribute the observed features to *g*-derived modes that are made weakly allowed by perturbations that break the inversion symmetry, e.g., finite chain lengths or chain branching. For the region 300–400 cm^{-1}, we find, just as for the dimer and *R* polymer, fewer measured than calculated peaks. This is likely due to the weakness of the experimental intensities.

Between 500 and 620 cm^{-1}, the *O*-polymer spectrum is very complex. As a result, our *O*-polymer mode assignments in this region are more tentative than for the other polymerized structures. We assign the most conspicuous features (Table IV) based on the QMD calculations and on a comparison with the *R*-polymer and dimer spectra. For example, the strong multiplet of peaks between 520 and 532 cm^{-1} resembles the dimer feature consisting of $T_{1u}(1)$- and

$H_u(2)$-derived vibrations, and the intense peak at 613 cm^{-1} is similar to the *R*-polymer vibration at 610 cm^{-1}. We identify the *O*-polymer modes accordingly and find them consistent with the strong splittings predicted for $T_{1u}(2)$ and $H_u(2)$. As in the *R* polymer, the appearance of a $H_u(2)$-derived vibration at 613 cm^{-1} strongly supports the calculations and cannot be assigned if a weak distortion of the ball is assumed.[27]

A large number of reproducible *O*-polymer modes remain unassigned (listed in Ref. 55), resulting from an overabundance of features compared to the number of calculated vibrations in the 500–620-cm^{-1} region. One possible origin of these modes is the presence of other types of bonded structures along with the 1D linear chains, such as dimers, which are intermediate products in the low-pressure formation of the 1D polymer.[16,35] Although *O*-polymer features appear at many dimer mode frequencies, there is not a consistent appearance of all dimer modes in the *O*-polymer spectrum, so we can rule out heavy contamination. Alternatively, chain defects, such as chain ends with C_{2v} site symmetry or chain branching points with unknown symmetries, may activate more silent modes and shift the frequencies of observed modes, thus producing ''extra'' features in the observed spectrum. The similarity of our *O*-polymer spectrum to that of the solution-processed high-molecular-weight photopolymer[25] supports the hypothesis of defects in the linear chains. Neither chain defects nor other bonded structures (implying poor sample quality) are indicated in the x-ray diffraction studies, however,[37] leading to an impasse. On the other hand, good sample quality is consistent with Davydov splitting of modes, which was suggested as a possible explanation of unexpected splitting of $A_g(2)$ in RbC_{60}.[56] Obviously, the origin of the multitude of ''extra'' modes has important implications for our understanding of the sample quality, and vice versa.

As a final note, we point out that the complex FIR vibrational structure of the *O* polymer contrasts sharply with that of the linear polymer, RbC_{60}, which exhibits a clean spectrum of six peaks in the 500–600-cm^{-1} region.[5,24] We find that features at 509, 517, 526, 541, 554, and 571 cm^{-1} also appear in the *O*-polymer spectrum, but with much weaker intensity than the primary modes we assign. Interestingly, whereas the FIR spectra of the *O* polymer and RbC_{60} differ considerably, the Raman spectra of the two linear polymers were found to be nearly identical.[51,56] Further investigation is under way.

V. CONCLUSION

In summary, we have made high-resolution transmittance measurements and quantum molecular-dynamics calculations of the FIR vibrational properties of the rhombohedral and orthorhombic HPHT C_{60} polymers and the $2+2$ cycloaddition C_{60} dimer. We find both experimental and theoretical evidence for wide splittings and large frequency shifts of I_hC_{60} modes due to distortion and symmetry reduction of the fullerene balls. The appearance of a feature near 610 cm^{-1} in the spectrum of each polymerized structure provides independent experimental evidence of a large frequency shift due to significant distortion, since this feature is located far from all fundamental modes of I_hC_{60}. We calculate unprecedentedly large downshifts for $T_{1u}(2)$-derived modes and extremely large splittings (as much as ≈ 100 cm^{-1}) of other modes. These downshifts and splittings are consistent with the experimental spectra. For the *R* and *O* polymers, the $T_{1u}(2)$-derived modes that are polarized in the stretched (bonding) direction are calculated to downshift below any $T_{1u}(1)$-derived vibrations. In contrast to the behavior of $T_{1u}(2)$, we observe narrow splitting and negligible shifts of $T_{1u}(1)$-derived modes in the *O* polymer and dimer in both experimental and theoretical spectra. Final confirmation of all assignments awaits the availability of single crystals of these structures for polarized FIR measurements. Our experimental data also confirm the expected D_{3d} and D_{2h} symmetries in the *R* polymer and dimer, based on the expected number of modes activated by symmetry reduction. The *O*-polymer spectrum does not allow such confirmation, due to an overabundance of unidentified modes, the origin of which is under investigation.

ACKNOWLEDGMENTS

We are grateful to the Division of Materials Research of the National Science Foundation (Grants No. 9623221 and 9624102), the Division of International Programs of the National Science Foundation (Grant No. INT-9722488), the Hungarian National Science Foundation (Grant No. OTKA T22404), the Japan Society for the Promotion of Science (RFTF96P00104, MPCR-363/96-03262), and the Grant-in Aid for Scientific Research on Priority Area ''Fullerenes and Nanotubes'' from the Japanese Ministry of Education, Science, Sports, and Culture for their generous support of this research. We thank G. Oszlányi for x-ray diffraction measurements of the orthorhombic polymer sample, and H. Kuzmany for useful discussions.

[1] W. Krätschmer, K. Fostiropoulos, and D. Huffman, Chem. Phys. Lett. **170**, 167 (1990).

[2] M. S. Dresselhaus, G. Dresselhaus, and P. C. Eklund, *Science of Fullerenes and Carbon Nanotubes* (Academic Press, New York, 1996).

[3] A.M. Rao, Ping Zhou, Kai-An Wang, G.T. Hager, J.M. Holden, Ying Wang, W.-T. Lee, Xiang-Xin Bi, P.C. Eklund, D.S. Cornett, M.A. Duncan, and I.J. Amster, Science **259**, 955 (1993).

[4] Y. Iwasa, T. Arima, R.M. Fleming, T. Siegrist, O. Zhou, R.C. Haddon, L.J. Rothberg, K.B. Lyons, H.L. Carter, Jr., A.F. Hebard, R. Tycko, G. Dabbagh, J.J. Krajewski, G.A. Thomas, and T. Yagi, Science **264**, 1570 (1994).

[5] M.C. Martin, D. Koller, A. Rosenberg, C. Kendziora, and L. Mihaly, Phys. Rev. B **51**, 3210 (1995).

[6] G. Oszlányi, G. Bortel, G. Faigel, L. Gránásy, G.M. Bendele, P.W. Stephens, and L. Forró, Phys. Rev. B **54**, 11 849 (1996).

[7] G.-W. Wang, K. Komatsu, Y. Murata, and M. Shiro, Nature (London) **387**, 583 (1997).

[8] S. Pekker, A. Jánossy, L. Mihaly, O. Chauvet, M. Carrard, and L. Forró, Science **265**, 1077 (1994).

[9] P.W. Stephens, G. Bortel, G. Faigel, M. Tegze, A. Jánossy, S. Pekker, G. Oszlányi, and L. Forró, Nature (London) **370**, 636 (1994).

[10] R. Moret, P. Launois, P.-A. Person, and B. Sundqvist, Europhys.

Lett. **40**, 55 (1997).
[11] G. Oszlányi, G. Baumgartner, G. Faigel, and L. Forró, Phys. Rev. Lett. **78**, 4438 (1997).
[12] V.D. Blank, S.G. Buga, G.A. Dubitsky, N.R. Serebrynaya, M.Y. Popov, and B. Sundqvist, Carbon **36**, 319 (1997).
[13] T. Pusztai, G. Oszlányi, G. Faigel, K. Kamarás, L. Gránásy, and S. Pekker, Solid State Commun. **111**, 595 (1999).
[14] S. Lebedkin, A. Gronov, S. Giesa, R. Gleiter, B. Renker, H. Rietschel, and W. Krätschmer, Chem. Phys. Lett. **285**, 210 (1998).
[15] B. Burger, J. Winter, and H. Kuzmany, Synth. Met. **86**, 2329 (1997).
[16] V.A. Davydov, L.S. Kashevarova, A.V. Rakhmanina, V.M. Senyavin, V. Agafonov, R. Ceolin, and H. Szwarc, Pis'ma Zh. Éksp. Teor. Fiz. **60**, 881 (1998) [JETP Lett. **68**, 928 (1998)].
[17] Y. Iwasa, K. Tanoue, T. Mitani, A. Izuoka, T. Sugawara, and T. Yagi, Chem. Commun. (Cambridge) **1998**, 1411 (1998).
[18] B. Sundqvist, Adv. Phys. **48**, 1 (1999).
[19] Recent structural studies have shown that the space groups of KC_{60} and RbC_{60} are different due to different chain orientations. Only KC_{60} is structurally analogous to the *O* polymer [P. Launois, R. Moret, J. Hone, and A. Zettl, Phys. Rev. Lett. **81**, 4420 (1998)].
[20] G.M. Bendele, P.W. Stephens, K. Prassides, K. Vavekis, K. Kordatos, and K. Tanigaki, Phys. Rev. Lett. **80**, 736 (1998).
[21] H. Kuzmany, R. Winkler, and T. Pichler, J. Phys.: Condens. Matter **7**, 6601 (1995).
[22] A.M. Rao, P.C. Eklund, J.-L. Hodeau, L. Marques, and M. Núñez-Regueiro, Phys. Rev. B **55**, 4766 (1997).
[23] V.A. Davydov, L.S. Kashevarova, A.V. Rakhmanina, V. Agafonov, H. Allouchi, R. Ceolin, A.V. Dzyabchenko, V.M. Senyavin, and H. Szwarc, Phys. Rev. B **58**, 14 786 (1998).
[24] K. Kamarás, Y. Iwasa, and L. Forró, Phys. Rev. B **55**, 10 999 (1997); **57**, 5543 (1998).
[25] B. Ma, A.M. Milton, and Y.-P. Sun, Chem. Phys. Lett. **288**, 854 (1998).
[26] J. Onoe and K. Takeuchi, Phys. Rev. B **54**, 6167 (1996).
[27] V. C. Long, J. L. Musfeldt, K. Kamarás, Y. Iwasa, and W. E. Mayo, Ferroelectrics (in press).
[28] G.B. Adams, J.B. Page, O.F. Sankey, and M. O'Keefe, Phys. Rev. B **50**, 17 471 (1994).
[29] M.R. Pederson and A.A. Quong, Phys. Rev. Lett. **74**, 2319 (1995).
[30] D. Porezag, M. Pederson, Th. Frauenheim, and Th. Kóhler, Phys. Rev. B **52**, 14 963 (1995).
[31] K. Esfarjani, Y. Hashi, J. Onoe, K. Takeuchi, and Y. Kawazoe, Phys. Rev. B **57**, 223 (1998).
[32] J. Menéndez and J. Page, in *Light Scattering in Solids, VIII*, edited by M. Cardona and G. Güntherodt (Springer, Heidelberg, 2000), p. 27.
[33] G.B. Adams and J.B. Page, in *Fullerene Polymers and Fullerene-Polymer Composites*, edited by P.C. Eklund and A.M. Rao (Springer-Verlag, Berlin, in press).
[34] P.A. Persson, O. Andersson, P. Jacobsson, A. Soldatov, B. Sundqvist, and T. Waägberg, J. Phys. Chem. Solids **58**, 1881 (1997).
[35] V.A. Davydov, L.S. Kashevarova, A.V. Rakhmanina, V. Agafonov, H. Allouchi, R. Ceolin, A.V. Dzyabchenko, V.M. Senyavin, H. Szwarc, T. Tanaka, and K. Komatsu, J. Phys. Chem. B **103**, 1800 (1999).
[36] M.E. Kozlov, M. Tokumoto, and K. Yakushi, Synth. Met. **86**, 2349 (1997).
[37] G. Oszlányi (unpublished).
[38] Y. Iwasa (unpublished).
[39] Paraffin is clear in the far infrared except for a narrow feature at 79 cm^{-1}.
[40] V.C. Long, J.L. Musfeldt, K. Kamarás, A. Schilder, and W. Schütz, Phys. Rev. B **58**, 14 338 (1998).
[41] O.F. Sankey and D.J. Niklewski, Phys. Rev. B **40**, 3979 (1989).
[42] G.B. Adams, J.B. Page, O.F. Sankey, K. Sinha, J. Menéndez, and Huffman, Phys. Rev. B **44**, 4052 (1991); G.B. Adams, O.F. Sankey, J.B. Page, M. O'Keeffe, and D.A. Drabold, Science **256**, 1792 (1992).
[43] G.B. Adams, J.B. Page, M. O'Keeffe, and O.F. Sankey, Chem. Phys. Lett. **228**, 485 (1994); J.R. Fox, G.P. Lopinski, J.S. Lannin, G.B. Adams, J.B. Page, and J.E. Fischer, *ibid.* **249**, 195 (1996).
[44] G.B. Adams, M.O'Keeffe, O.F. Sankey, and J.B. Page, *Novel Forms of Carbon*, edited by C.L. Renschler, J.J. Pouch, and D.M. Cox (Materials Research Society, Pittsburgh, 1993), p. 103; M. O'Keeffe, G.B. Adams, and O.F. Sankey, Phys. Rev. Lett. **68**, 2325 (1992); G.B. Adams, O.F. Sankey, J.B. Page, and M. O'Keeffe, Chem. Phys. **176**, 61 (1993); G.B. Adams, M. O'Keeffe, A.A. Demkov, O.F. Sankey, and Y.M. Huang, Phys. Rev. B **49**, 8048 (1994).
[45] For the *O*-polymer simulation, we used two special *k* points (Ref. 46) in the 1D Brillouin zone, and for the *R*-polymer simulation we used four special *k* points in the 2D zone.
[46] H.J. Monkhorst and J.D. Pack, Phys. Rev. B **13**, 5188 (1976).
[47] W.G. Fateley, F.R. Dollish, N.T. McDevitt, and F.F. Bentley, *Infrared and Raman Selection Rules for Molecular and Lattice Vibrations: The Correlation Method* (Wiley-Interscience, Sussex, UK, 1972).
[48] Table I does not show the low-frequency interball modes of the dimer $(A_g+B_{2g}+B_{3g}+A_u+B_{2u}+B_{3u})$, of which the B_{2u} and B_{3u} symmetry vibrations are expected to be IR active.
[49] B. Chase, N. Herron, and E. Holler, J. Phys. Chem. **96**, 4262 (1992).
[50] B. Burger, J. Winter, and H. Kuzmany, Z. Phys. B: Condens. Matter **101**, 227 (1996).
[51] B. Renker, H. Schober, R. Heid, and P.v. Stein, Solid State Commun. **104**, 527 (1997).
[52] G.B. Adams and J.B. Page (unpublished).
[53] J. Menéndez and S. Guha, in *22nd International Conference on the Physics of Semiconductors*, edited by D. Lockwood (World Scientific, Vancouver, Canada, 1994), p. 2093.
[54] For example, the combination of odd and even derivatives of $H_g(1)$ is allowed in the IR spectrum, according to selection rules.
[55] The following *O*-polymer features are unidentified: 450, 460, 465, 470, 480, 485, 510, 517, 532, 535, 538, 539, 544, 546, 548, 552, 558, 561, 563, 568, 573, 576, 588, 605, 608, and 610 cm^{-1}.
[56] J. Winter, H. Kuzmany, A. Soldatov, P.-A. Persson, P. Jacobsson, and B. Sundqvist, Phys. Rev. B **54**, 17 486 (1996).